processes

MDPI

Article

Control Strategy Based on Artificial Intelligence for a Double-Stage Absorption Heat Transformer

Suset Vázquez-Aveledo [1], Rosenberg J. Romero [2,*], Moisés Montiel-González [3] and Jesús Cerezo [2]

[1] Postgraduate in Science, Autonomous University of Morelos State, Av. Universidad 1001, Cuernavaca 62209, Morelos, Mexico; suset.vazquez@uaem.edu.mx
[2] Engineering and Applied Research Centre, CIICAp, Autonomous University of Morelos State, Av. Universidad 1001, Cuernavaca 62209, Morelos, Mexico; jesus.cerezo@uaem.mx
[3] Facultad de Ciencias Químicas e Ingeniería, FCQeI, Autonomous University of Morelos State, Av. Universidad 1001, Cuernavaca 62209, Morelos, Mexico; moises.montiel@uaem.mx
* Correspondence: rosenberg@uaem.mx; Tel.: +52-777-329700 (ext. 6233)

Abstract: Thermal energy recovery systems have different candidates to mitigate CO_2 emissions as recommended by the UN in its list of SDGs. One of these promising systems is thermal absorption transformers, which generally use lithium-water bromide as the working fluid. A Double Stage Heat Transformer (DSHT) is a thermal machine that allows the recovery of thermal energy at a higher temperature than it is supplied through the effect of steam absorption in a concentrated solution of lithium bromide. There are very precise thermodynamic models which allow us to calculate all the possible operating conditions of the DSHT. To perform the control of these systems, the use of Artificial Intelligence (AI) is proposed with two computational techniques—Fuzzy Logic (FL) and Artificial Neural Network (ANN)—to calculate in real-time the set of variables that maximize the product's Gross Temperature Lift (GTL) and Coefficient of Performance (COP) in a DSHT. The values for Coefficient of Determination (R^2), Mean Square Error Root (MRSE), and Mean Error Bias (MBE) for the two types of computational techniques were analyzed and compared with the purpose of identifying which of them may be more accurate to calculate the operating conditions (temperatures, pressures, concentration and flows) with the highest COP for an interval of the value of the temperature absorption entered by the user. The result of the analysis of the evaluated techniques concluded that the control strategy of a DSHT in real-time will be based on the precise calculation of the refrigerant flow in the second evaporator with a Neural Network of 30 neurons, 300 weights and 40 bias, as it is more accurate than the Fuzzy Logic technique. The goodness-of-fit for two computational techniques was evaluated as having an R^2 higher than 0.98 for the provided data. Future AI controllers must be based on evaporator flow values with evaporator power at 3.9^{-04} kg/KJ.

Keywords: absorption heat transformer; heat pump; artificial neural network; fuzzy logic; artificial intelligence; aqueous lithium bromide

Citation: Vázquez-Aveledo, S.; Romero, R.J.; Montiel-González, M.; Cerezo, J. Control Strategy Based on Artificial Intelligence for a Double-Stage Absorption Heat Transformer. *Processes* **2023**, *11*, 1632. https://doi.org/10.3390/pr11061632

Academic Editor: Jie Zhang

Received: 25 April 2023
Revised: 19 May 2023
Accepted: 24 May 2023
Published: 26 May 2023

1. Introduction

Energy consumption plays an important role in the development of the daily activities of human beings. This consumption comes mainly from fossil resources, which triggers major environmental problems such as greenhouse gas (GHG) emissions mainly responsible for climate change. One of these is carbon dioxide (CO_2) resulting from the burning of fuels and industrial processes, which increased by 0.9% from 2021 to 2022, reaching a new all-time high of 36.8 Gt [1].

The industrial sector is one of the largest energy consumers [2], generating high amounts of waste heat and promoting thermal pollution. The recovery of this waste heat allows its reuse in other processes in the industry, and this means great energy savings [3].

The innovation of technologies to recover waste heat is of great importance today because it represents a method of using the unused energy produced in the industry. One of these technologies used for heat recovery is absorption systems, specifically, Single-Stage Heat Transformers (SSHT), which are a type of heat pump that could take advantage of waste heat from an industrial process or a low-quality source and bring a part of it to a higher temperature in order to use it for a specific purpose [4].

Absorption Heat Transformer (AHT) are thermodynamically efficient equipment, with low environmental impact and can be adapted to renewable energies such as solar or geothermal energy [4–6]. These devices have demonstrated feasibility for water purification applications, [7–14], which could directly affect Sustainable Development Goal No. 6 of the UN 2030 Agenda: Clean Water and Sanitation.

Studies have produced many findings on the feasibility of adapting these systems to industrial processes, either for heat recovery in a secondary process or for the re-entry of heat into the process and reduction in energy requirements [15–23].

The absorption systems of type II (or inverse) work in a thermodynamic cycle with four-unit operations: generation, condensation, evaporation, and absorption. Heat exchange occurs in all of these, and simultaneous exchange of matter and heat occurs in two; with variables of temperature, pressure, concentration, power, and flow of fluids at different densities, it is a complex process. In addition, this equipment cannot be self-controlled; if there are not trained personnel operating this type of equipment, it can suffer deterioration due to overheating [24]. This implies that the system cannot operate on its own under the most favorable conditions such as a non-crystallization zone, a zone with different pressures, and/or without condensate flow. These three conditions lead to the thermodynamic cycle being inhibited or not operating. The increase in pressure in the upper area of this equipment can cause overheating—generating chemical risks for operators—and deterioration or destruction of the equipment.

On the other hand, these absorption systems operate with a working mixture that is a combination of a working fluid (refrigerant) and an absorbent. Therefore, the behavior of the absorption cycle depends on the thermodynamic properties of the local conditions; the physicochemical conditions of both the working fluid and the absorbent are unique within each component where one of the unit operations of the cycle occurs. Among the most used working mixtures for SSHTs are the mixtures water–lithium bromide (H_2O–LiBr) and water–Carrol, which is a mixture of water with lithium bromide and ethylene glycol as an additive to increase the concentration of operation up to 70% instead of only the 60% of the original [25].

The operation of the thermodynamic cycle is influenced by disturbances in the operation associated with the temperature of the environment [26]; these disturbances are measurable but not controllable, and limit the performance of the condenser as it necessarily requires the exchange of temperature with the environment. Therefore, the condenser is subject to environmental conditions causing variations in the pressure and concentration of the desorber.

Based on the above, the existing problem is related to the automated control of a Double-Stage Heat Transformer (DSHT), which leads to the development of an automatic control strategy applied to this equipment capable of involving all the variables present in the system as well as disturbances in these variables. The literature presents several works related to the automatic control of heat pumps by mechanical compression and, to a lesser extent, by type I absorption [27]. However, for SSHT, the few reported works on control depending on the energy to be revalued are based only on the classic Proportional, Integrative and Derivative control (PID), not centralized and without the feedback of the variables that optimize the performance of the cycle.

A previous controlled system with similar heat transfer processes is the mechanical vapor compression heat pump. These systems have on/off control and several studies have reported on them. Other authors have published research on the application of PID to

pumps of heat by compression, among which are the works of [28–30]. Another author [31] has used PID control to obtain a maximum COP of the system at a fixed set of temperatures.

The technological development of instrumentation for control, as well as computational advances, has improved the progress of more advanced control concepts and strategies based on AI models. Another author [32] employed a diffuse self-tuning control method–PID to regulate PID parameters in line and maintain refrigerant flow in an appropriate range of a compression cycle. Experimental results show improvements in this method compared to that of the conventional PID control system. Another publication [33] tested three different control algorithms—PID, FL and ANN—in a mechanical vapor compression cooling system. It was found that the ANN control algorithm gave a more robust response to the disturbance effect in the system.

As for absorption heat pumps, the published studies only focus on control strategies applied to type I. Another author [34] demonstrated the performance of a PI feedback loop in regulating generation temperature in a car-exhaust-driven water and ammonia system. Goyal [35] developed a model-based P control (the control output is proportional to the error at all times) and PI control (the control output is proportional to the integrative of the error) control of a natural-gas-powered ammonia–water absorption chiller for control. The results indicated an improvement in COP of approximately 8–10% under variable ambient temperature operating conditions. These authors [36] also achieved feedback control of the temperature of the cooled water supply by varying the mass flow rate of relatively hot recycled water in a lithium bromide–water absorption chiller.

Xu et al. [37] implemented a PID controller in a lithium bromide water–bromide chiller simulation using two approaches: The first used the temperature of the chilled water supply as the controlled variable and the flow rate of the generator heat source as the manipulated variable. The second approach only used generation temperature as a controlled variable. The system demonstrated constant COP and fast control with the temperature of the generator solution as the control variable.

Garciadealva et al. [38] proposes a cascade control system with PID controllers applied to a single-stage absorption cooling system operated with solar energy and the ammonia–water mixture. The applied control improved the thermodynamic steady state and the response for all times.

In the literature review, several automatic control strategies have been presented for mechanical compression and absorption heat pumps, both type I; however, for type II heat pumps (SSHT and DSHT), it is practically nil. As mentioned, the publications concerning automatic SSHT control are based on PID, that is, a type of non-centralized control that—in the case of an absorption system consisting of a thermodynamic cycle—does not guarantee maximum heat recovery. A theoretical correlation strategy was proposed with a PID control that uses the flow ratio for a DSHT with a water–Carrol mixture [39].

The need arises to develop a strategy for automatic control of a DSHT operating with water–lithium bromide with the purpose of calculating the refrigerant flow for the maximum value of COP and GTL, which guarantees the recovery of the thermal energy of the system with the greatest efficiency for a selected operation condition. For this, the implementation of intelligent control is carried out, with the evaluation of two computational techniques associated with Artificial Intelligence, in a certain way that is autonomous, nonlinear, and learning [40], the nonlinearity of which corresponds well to thermodynamic models [41].

The intelligent control applied to this type of multivariable and non-linear system allows using centralized rules that can be varied for the case of this cycle, because the aqueous lithium bromide enthalpies are nonlinear functions of temperature and weight concentration; the AI can work more effectively compared to setting only one of the variables with PID systems because, unlike isolated controls for several variables (not central), they lead to a set of actions for one full cycle of control.

The objective of this article is to show a multivariable automatic control strategy with previously referenced Artificial Intelligence techniques for DSHT control that works with

the water–lithium bromide mixture [17] for which theoretical and experimental data are available. The proposal DSHT control strategy will be calculated by controlling refrigerant flows based on flow ratio calculation research [39] in both stages, and the main objective is to calculate with AI the absorption temperature in the second stage—which has the higher COP multiplied by GTL product value—that is the best operating condition.

2. Materials and Methods

An AHT is a reverse heat pump or a type II heat pump and, it can be classified as simple-effect or advanced. It can operate with conventional or alternative mixtures. The components of an AHT are heat exchangers: a Generator (GE), a Condenser (CO), an Evaporator (EV) and an Absorber (AB).

2.1. Absorption Cycle

2.1.1. Single-Stage Heat Transformer (SSHT)

The cycle of an SSHT is shown on a pressure–temperature diagram in Figure 1. It is observed that the SSHT operates with two pressure levels and three temperature levels where the same waste heat is supplied to the Generator and Evaporator. In the case of SSHT and DSHT systems, the working fluid and the absorbent are the water and the aqueous lithium bromide, respectively, which revalue the energy supplied in the Evaporator and Generator.

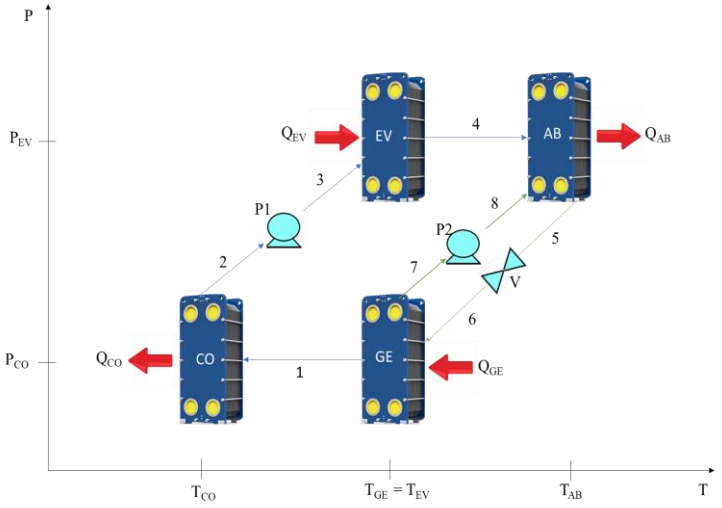

Figure 1. Diagram of the cycle of an SSHT within the coordinates of pressure and temperature.

The cycle begins by adding heat (waste, geothermal, solar) to the Generator (Q_{GE}) and the Evaporator (Q_{EV}), which can have a relatively intermediate temperature (60–80 °C). In the Generator is the concentrated mixture of lithium bromide and the refrigerant (also called working fluid); part of the working fluid (water) is evaporated as a product of the heat exchange with the waste source, and then it is sent to the Condenser where it changes to a liquid phase by disbursing an amount of heat (Q_{CO}) to the environment.

The working fluid or condensed refrigerant is water, and it is sent by a pump to the Evaporator where it receives an amount of heat to again pass to the vapor phase, but at a higher pressure, and then is conducted to the Absorber where it is absorbed by the aqueous mixture of concentrated lithium bromide coming from the Generator, releasing an amount of useful heat (Q_{AB}) at the highest relative temperature of the cycle (greater than 80 °C). Finally, the diluted fluid into the Absorber is sent (through a valve to the zone of lower pressure) to the Generator to restart the cycle again [4].

2.1.2. Double-Stage Heat Transformer (DSHT)

A double-stage AHT is the combination of two single-stage heat transformers, resulting in a device containing a total of 8 heat exchangers, 4 for each stage, as shown in Figure 2.

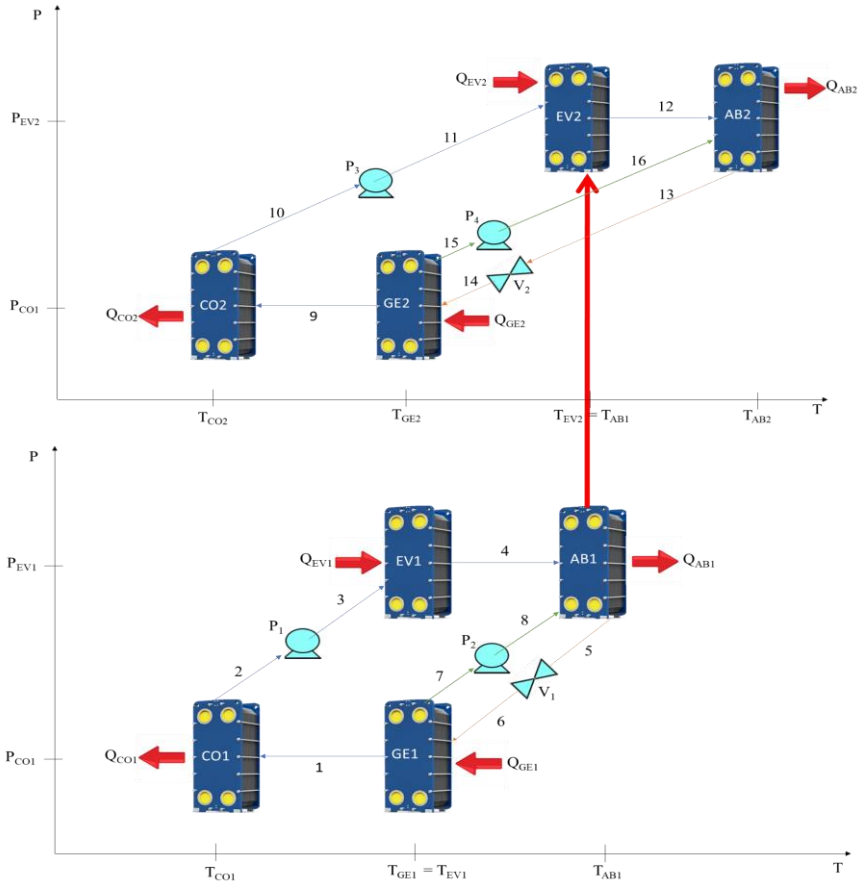

Figure 2. Diagram of the cycle of a DSHT within the coordinates of pressure and temperature.

In a Double-Stage Heat Transformer (DSHT), the heat transferred to the stage 1 Absorber is used to power the stage 2 Evaporator, while the heat generated from stage 2 is also fed by the same heat source that feeds the stage 1 Generator and stage 1 Evaporator. In Evaporator 2, the working fluid or refrigerant (water) from the stage 2 Condenser (at near-ambient temperature) is evaporated at a higher pressure and temperature value than the stage 1 Evaporator, allowing the useful heat obtained in stage 2 in the Absorber to have a higher temperature value compared to the stage 1 Absorber [39].

The main parameters of these thermal parameters are COP, Flow Ratio (FR) and GTL and are defined below for each cycle:

- COP can be defined as the heat recovery capacity or the efficiency of transformation of useful heat with respect to the one supplied, as in Equations (1) and (2):

$$COP_{SSHT} = \frac{Q_{AB1}}{Q_{GE1} + Q_{EV1} + WP_1 + WP_2}, \quad (1)$$

$$COP_{DSHT} = \frac{Q_{AB2}}{Q_{GE1} + Q_{GE2} + Q_{EV1} + WP_1 + WP_2 + WP_3 + WP_4}, \quad (2)$$

where WP_i is the work done by pump number i (1 to 4), which—according to the literature—is less than 5% and, in most conditions, its effect on the COP can be neglected [41].

- GTL is defined as the difference between the temperature of the Absorber (T_{AB}) and Evaporator (T_{EV}), as in Equations (3) and (4):

$$GTL_{SSHT} = T_{AB1} - T_{EV1}, \quad (3)$$

$$GTL_{DSHT} = T_{AB2} - T_{EV1}, \quad (4)$$

- FR is a dimensionless value that is defined as the ratio between the concentration of the concentrated solution of lithium bromide in the Generator (X_{GE}) divided by the difference in concentrations of concentrated and diluted lithium bromide in the Generator and Absorber ($X_{GE} - X_{AB}$), respectively, and is equivalent to the ratio between the flow of the dilution solution in lithium bromide with the ratio to the working fluid or refrigerant fluid, as per Equations (5)–(8):

$$FR_{SSHT} = \frac{X_{GE1}}{X_{GE1} - X_{AB1}}, \quad (5)$$

$$FR_{SSHT} = \frac{m_{AB1}}{m_{EV1}}, \quad (6)$$

$$FR_{DSHT} = \frac{X_{GE2}}{X_{GE2} - X_{AB2}} \quad (7)$$

$$FR_{DSHT} = \frac{m_{AB2}}{m_{EV2}}, \quad (8)$$

According to previous research [26], it was concluded that a temperature change in the SSHT Condenser generates a change in the other components of the cycle. That is, a change in temperature in the Condenser causes pressure changes in the areas of low relative pressure, causing changes in fluid concentration with a high concentration of lithium bromide (X_{GE}). In addition to this, [39] concludes that a change in concentration produces a change in the flow ratio (FR) and therefore in the value of the flows of the evaporates and the Absorber in the first instance and later in the Generator (conservation of matter); these changes are limited by the conditions of thermodynamic equilibrium. The equilibrium values include pressure, temperature, and concentration; the theoretical and experimental values of FR correspond exactly to concentration and flux changes as seen in Equations (5) and (7) for SSHT and (6) and (8) for DSHT. A change in X_{GE} implies a change in the flows of the whole cycle.

The thermodynamic operating data of an SSHT with lithium bromide were calculated and are shown in Figure 3. This figure shows the behavior of the COP_{SSHT} as a function of the GTL_{SSHT} for different temperatures indicated for each component. The Generator operates with a constant temperature value at 50 °C, the Condenser temperature was varied from 20 °C to 25 °C, the absorption temperature has been calculated for a range of 70 °C to 75 °C and the evaporation temperature was varied from 45 °C to 50 °C. It is also observed that with increasing GTL_{SSHT}, the COP_{SSHT} decreases nonlinearly, obtaining the largest COP_{SSHT} for small values of $GTL_{SSHT.}$

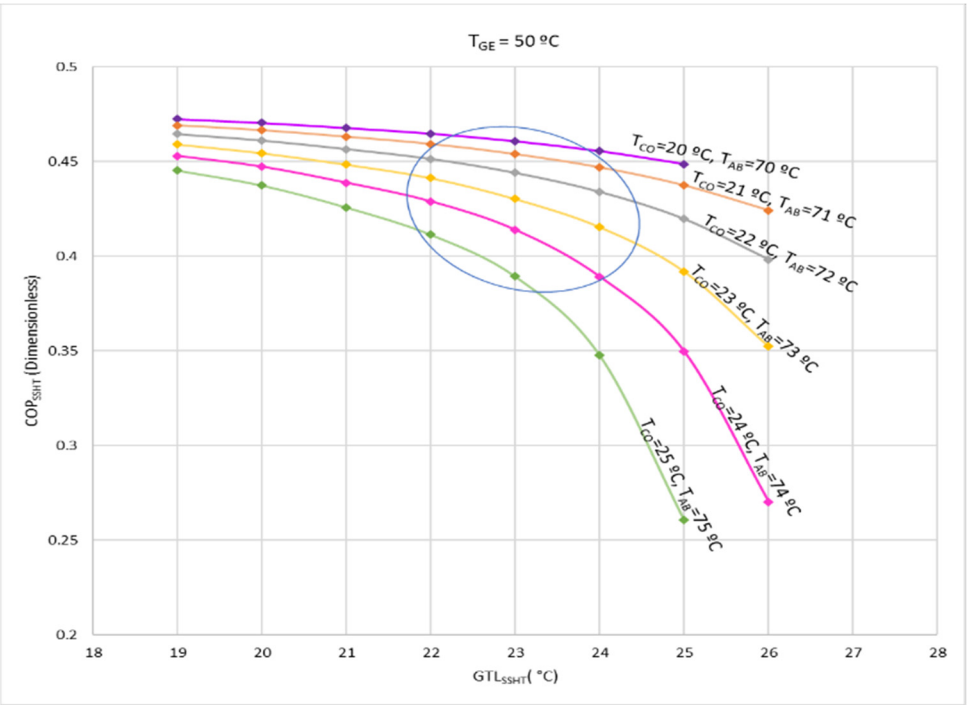

Figure 3. The behavior of the COP_{SSHT} as a function of GTL_{SSHT} for the mixture water–lithium bromide.

According to the study carried out, in an SSHT cycle [41] the maximum values of the COP_{SSHT} implies the lowest value of GTL_{SSHT}, as can be seen in the upper left part of Figure 3. In addition, the highest values of GTL_{SSHT} are obtained in the minimum values of COP_{SSHT} for each T_{AB} between 70 and 75 °C. Maximum values of COP_{SSHT} or maximum values of GTL_{SSHT} are not the best scenarios to consider as a control strategy. It is then proposed as an objective function to find the maximum value of both to guarantee the best operation of the SSHT without having to diminish either of the two parameters; for this, the artificial variable to be maximized is the product of the COP by the GTL (in both stages). In addition to this, Figure 3 shows the area of the conditions where the highest values of the COP_{SSHT} x GTL_{SSHT} product marked within an oval are obtained, so two Artificial Intelligence (AI) computing techniques are compared to determine which of them is more accurate in the calculation of the M_{EV} (at each stage) for a T_{AB} and set of GTL values.

2.2. Artificial Intelligence

The control strategy that will be implemented to operate the DSHT in the conditions of the higher COP multiplied by GTL product will obtain a value of M_{EV} from the use of Artificial Intelligence. Two AI computer programs were first developed for an SSHT to determine which of the two (Fuzzy Logic and Neural Networks) is more accurate for system stabilization. Figure 4 shows a schematic of the general AI model, which presents 5 input variables defined by a thermodynamic model of the cycle [41] and 5 output variables of interest for the evaluation of Q_{EV}, Q_{GE}, X_{GE}, FR and M_{EV}, being a MIMO (multiple-input and multiple-output) system. The COP is a function of the powers calculated as outputs of the program, as indicated by Equation (1). The GTL is calculated based on the T_{AB} (which is not fixed); during the calculation process, all temperatures ($T_{EV,}$ $T_{GE,}$ T_{CO}) have a domain or interval of interest that can be assigned. The value of the GTL_{SSHT} will depend on the output values T_{AB} and $T_{EV.}$ Therefore, the GTL_{SSHT} multiplied by COP_{SSHT} product is known for those intervals. The names and units of measurement of inputs and outputs are shown in Table 1.

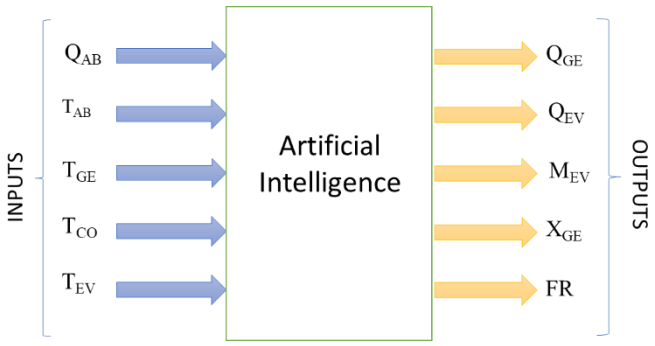

Figure 4. Schematic of the computational model of AI.

Table 1. AI input and output variables.

Tickets	Outputs
Q_{AB}: Thermal power of the Absorber [kW]	Q_{GE}: Thermal power of the Generator [kW]
T_{AB}: Absorber temperature [°C]	Q_{EV}: Evaporator thermal power [kW]
T_{GE}: Generator temperature [°C]	M_{EV}: Working fluid flow [kg/s]
T_{CO}: Condenser temperature [°C]	X_{GE}: Generator concentration [%w]
T_{EV}: Evaporator temperature [°C]	FR: Flow ratio [Dimensionless]

The values of the output variables of the AI computer program for each input vector correspond to the values of a higher product of COP_{SSHT} multiplied by GTL_{SSHT}, and from this output value the values of the mass flows can be determined in the SSHT depending on the external power [41] that enters the Generator (Q_{GE_EX}) and Evaporator (Q_{EV_EX}), as per Equations (9) and (10):

$$Q_{GE\_EX} = M_{1\_sim} \times C_P \times (T_F - T_{GE\_S}) \quad (9)$$

$$Q_{EV\_EX} = M_{2\_sim} \times C_P \times (T_{GE\_S} - T_{EV\_S}), \quad (10)$$

where:

- Cp is the heat capacity of the fluid entering the Generator.
- T_F is the outlet temperature of the fluid that comes from a heat source after passing through the Generator.
- T_{GE_S} and T_{EV_S} are the temperature of a constant heat source from which energy is entered into the generation and evaporation processes.
- M_{1_sim}: is the flow of a heat source to the Generator (geothermal, solar, industrial waste).
- M_{2_sim}: is the flow of a heat source to the Evaporator (may be the same as the Generator).

2.2.1. Computational Model Using Fuzzy Logic

The Fuzzy Logic computational model is based on IF–THEN rules and is solved by a Fuzzy Logic controller (Figure 5) in four stages as listed below [42]:

1. Input variables can be words or sentences, which, through membership functions, are converted into linguistic variables.
2. The fuzzification generates a blurred output, that is, the sharp values are blurred for a fuzzy output.
3. The mechanisms of fuzzy inference have the task of interpreting the rules of type IF–THEN contained in the rule base of the physical phenomenon to obtain the output values from the current values of the linguistic variables input to the system as indicated by the program.
4. Defuzzification is the conversion of a diffuse quantity into a precise quantity. The output of a fuzzy process can be the logical union of two or more fuzzy membership functions defined in the discourse universe of the output variable. Among the

methods that have been proposed in the literature to perform the defuzzification stage is the centroid method, which is defined by Equation (11) that determines the defuzzified × value [43]:

$$x = \frac{\sum_{i=1}^{n} x_i \mu(x_i)}{\sum_{i=1}^{n} \mu(x_i)} \quad (11)$$

where:

- n represents the number of items in the sample;
- x_i are the elements;
- $\mu(x_i)$ is the membership value for point x_i in the universe of discourse.

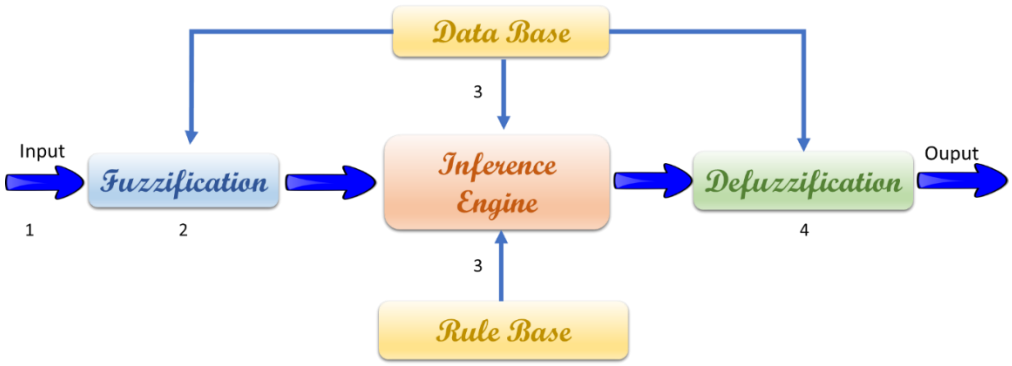

Figure 5. Fuzzy Logic controller.

The programming of the model based on Fuzzy Logic was developed using the MATLAB toolbox FIS (Fuzzy Inference System). This graphical interface allows users to create input–output variables and fuzzy sets as well as define the type of controller (Mandani or Sugeno), the base of fuzzy rules and other parameters of the inference process [44] that are consistent with what is proposed [42].

For the diffuse implication, the rule of the t-norm of the minimum was selected; for the aggregation, the rule of the s-norm of the maximum was chosen; and, for the diffusion, it was decided by the centroid method [45], which corresponds to physical phenomena that exhibit similarity with the absorption process.

In this work, once the input variables, output variables and fuzzy inference handler were determined, the MATLAB FIS editor was used to model the fuzzy sets. For the values of the output variables, a normalization of the data was performed [46]. Linguistic tags allow good interpretability to interact with experts on the phenomenon and adjust the mathematical model. Table 2 shows a description of these values:

Table 2. Universe of discourse and linguistic labels of input and output variables.

Title 1	Variables	Universe of Discourse	Language Tags
Tickets	Q_{AB} [kW]	1–2	[1-2]
	T_{CO} [°C]	20–25	[20-21-22-23-24-25]
	T_{AB} [°C]	70–75	[70-71-72-73-74-75]
	T_{GE} [°C]	50–55	[50-51-52-53-54-55]
	T_{EV} [°C]	45–50	[45-46-47-48-49-50]
Outputs	Q_{GE} [kW]	0–1	[0_0-0_1-0_2-0_3-0_4-0_5-0_6-0_7-0_8-0_9]
	Q_{EV} [kW]	0–1	[0_0-0_1-0_2-0_3-0_4-0_5-0_6-0_7-0_8-0_9]
	M_{EV} [kg/s]	0–1	[0_0-0_1-0_2-0_3-0_4-0_5-0_6-0_7-0_8-0_9]
	X_{GE} [%w]	0–1	[0_0-0_1-0_2-0_3-0_4-0_5-0_6-0_7-0_8-0_9]
	FR [dimensionless]	0–1	[0_0-0_1-0_2-0_3-0_4-0_5-0_6-0_7-0_8-0_9]

The membership functions (MFs) of input variables and output variables were selected with a representativeness criterion [47]. For this reason, triangular and trapezoidal functions were chosen for the input variables while triangular functions were used for the output variables. The absorption power (Q_{AB}) input variable was chosen as a trapezoidal MF and the other input variables were triangular and trapezoidal MFs. All output variables were chosen as triangular MFs. The domains of each partition were chosen to selected the operating conditions for each input variable, and for the output variables each partition responds to the GTL multiplied by COP higher product condition for an input condition with 5 variables.

The fuzzy rules base was implemented with the FIS rules editor (Figure 6), which combines the fuzzy values of the input variables with the logical operators AND or OR and the fuzzy inference system, in this case, the method of the t-norm of the minimum. In addition, each rule assigns values to the output variables. Figure 6 shows just a part of the first 17 rules in the FIS rules editor.

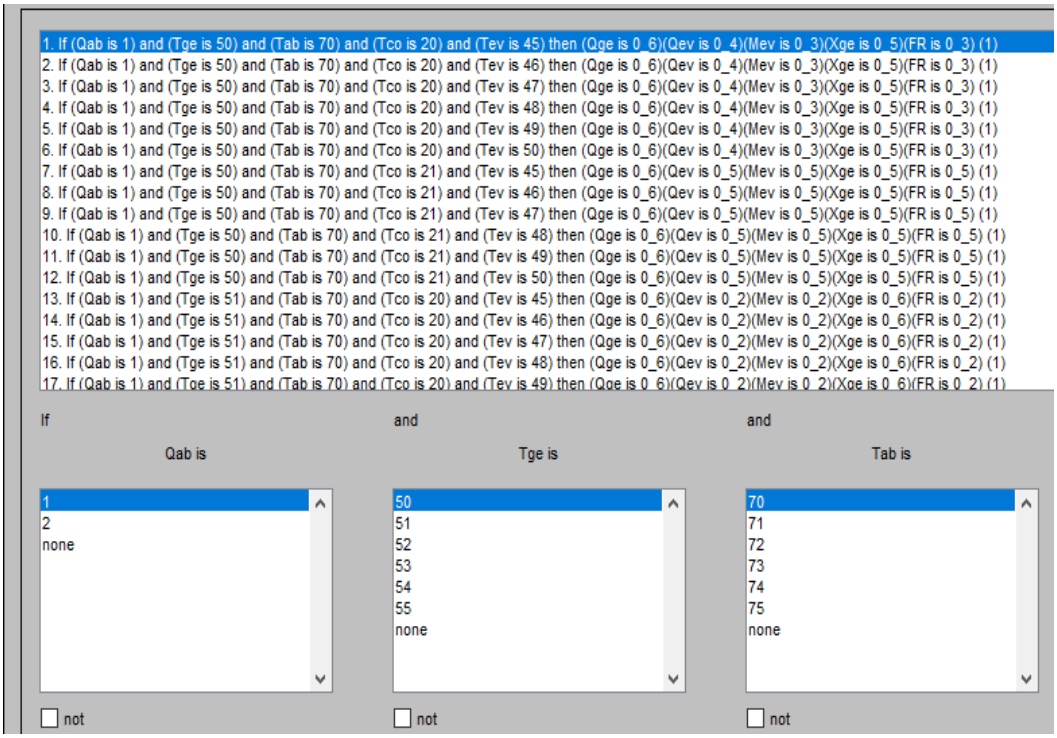

Figure 6. Screengrab of the first 17 FIS rules.

Example of 3 fuzzy rules:

1. If (Q_{AB} is 1) and (T_{AB} is 70) and (T_{GE} is 50) and (Tco is 20) and (T_{EV} is 45) then (Q_{GE} is 0_6) (Q_{EV} is 0_4) (M_{EV} is 0_3) (X_{GE} is 0_5) (FR is 0_3)

...

7. If (Q_{AB} is 1) and (T_{AB} is 70) and (T_{GE} is 50) and (Tco is 21) and (T_{EV} is 45) then (Q_{GE} is 0_6) (Q_{EV} is 0_5) (M_{EV} is 0_5) (X_{GE} is 0_5) (FR is 0_5)

...

13. If (Q_{AB} is 1) and (T_{AB} is 70) and (T_{GE} is 50) and (Tco is 22) and (T_{EV} is 45) then (Q_{GE} is 0_6) (Q_{EV} is 0_2) (M_{EV} is 0_2) (X_{GE} is 0_5) (FR is 0_6)

...

To complete a total of 2592 rules in which mapping of each membership function was made for all the others (data set available on request). The editing of all rules takes much time (close to 1 min per each rule), but the learning time in a portable PC with an Intel i7 © processor is lower than 1 s.

2.2.2. Computational Model using Neural Networks

Artificial Neural Networks are made up of four main elements: inputs, synaptic weights, activation function and output. The multi-layer perceptron network configuration or feed-forward is the structure used for an approximation function within supervised learning. The transfer functions used in the different layers and their neurons allow network learning to present linear and nonlinear relationships between input and output variables. Feed-forward networks in their structure present sigmoid functions in the hidden layers and linear functions in the output layer [48]. Figure 7 shows a generic schematic of a basic Artificial Neural Network of a feed-forward type.

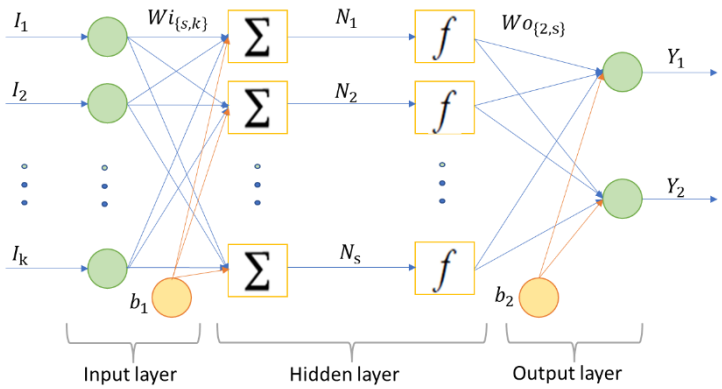

Figure 7. The basic structure of a feed-forward Neural Network.

The range of the input variables responds to the operating conditions analyzed for the AHT varied by 1 °C and for the values of the output variables a normalization of the data from 0.0 to 1.0 was performed. Table 3 shows the range of these values:

Table 3. Variables and values of input and output variables.

	Variables	Value
Inputs	Q_{AB} [kW]	1–2
	T_{CO} [°C]	20–25
	T_{AB} [°C]	70–75
	T_{GE} [°C]	50–55
	T_{EV} [°C]	45–50
	Q_{GE} [kW]	0–1
	Q_{EV} [kW]	0–1
Outputs	M_{EV} [kg/s]	0–1
	X_{GE} [%w]	0–1
	FR [dimensionless]	0–1

The learning algorithm of the selected Neural Network has as its main function the adjustment of the weights and bias of the network to ensure that the desired outputs are obtained with respect to the inputs by minimizing the error. To determine the number of neurons in each layer of the network configuration, as well as the number of layers to include, there is no method or rule that defines—nor there is an optimal number of neurons to solve—a particular problem, that is, the trial and error method is used [49]; in this study, the value that allows defining the number of neurons was based on the correlation between the values reproduced by the Artificial Intelligence Neural Network is greater than 0.99.

ANN programming was developed using the nftool (Neural Fitting) tool for MATLAB. MATLAB's nftool application is a graphical interface which allows you to select data and create and train a network, and it is possible to evaluate its performance using mean square error and regression analyses. The networks created by nftool are characterized by the following [44]:

- A hidden layer (the user can change the number of hidden units).
- Hidden units have a sigmoid activation function (tansig or logsig) while output units have a linear activation function.
- The training algorithm is Backpropagation based on a Levenberg–Marquardt minimization method.
- The learning process is controlled by a cross-validation technique based on a random division of the initial data set into 3 subsets: training (weight adjustment), control of the learning process (validation) and evaluation of the quality of the approach (testing).

The goodness of fit approximation can be assessed by the following [50]:

- Mean square error (MSE): expresses the difference between the correct outputs and those provided by the network; the approximation is better if MSE is smaller (closer to 0).
- Pearson Correlation Coefficient (R): measures the correlation between correct outputs and those provided by the network; the closer R is to 1, the better the approximation.

For this ANN-based computational program, there are 5 network input parameters and 5 output parameters. Different networks with different numbers of hidden neurons were used; the number of neurons ranged from 5 to 25. To train the networks, the input vectors and target vectors were randomly divided into three sets as follows: 70% were used for training, 15% were used to validate that the network is generalizing and the remaining 15% were used as a completely independent test of network generalization.

There is new model for pressure and temperature ANN; the literature has referred to other processes that use 70% for training, 20% for validation and just 10% for testing [51].

2.3. Validation of the Two Models

To verify the similarity of the data resulting from the computational models of Artificial Intelligence based on Fuzzy Logic and Neural Networks, for the data of the thermodynamic method, different deviation indicators were used to assess the goodness-of-fit between both sets of data for the two AI computational programs [52]. The deviation indicators are defined below:

- Deviation (%): allows you to see how far an approximate value is from an exact one.

$$Deviation(\%) = \frac{|X_{sim} - X|}{X}(\times 100), \tag{12}$$

where X_{sim} is each of the output values obtained in the two computational models studied.

- Mean square error root (RMSE): Measures the amount of error that exists between two sets of data, that is, it gives us a measure of how close the points of the observed data are to the estimated values. Near-zero values of RMSE indicate a better fit, and a value of RMSE = 0 indicates a perfect fit between the observed series and the estimated series.

$$RMSE = \sqrt{\frac{\sum_{i=1}^{N}\left(X_{sim,i} - X_i\right)^2}{N}} \tag{13}$$

where N represents the amount of data and X_i represents each of the values obtained in the thermodynamic model [53].

- Mean Error Bias (MBE): Used to validate model results against experimental data, it represents the degree of correspondence between a prediction and an observation, describing whether a model overestimates or underestimates the observation.

$$MBE = \frac{\sum_{i=1}^{N}\left(X_{sim,i} - X_i\right)}{N}, \tag{14}$$

- Coefficient of determination (R^2) indicates the goodness-of-fit of the model, and its limits are from 0 to 1; 0 indicates that the proposed model does not reproduce the data, and 1 indicates a perfect reproduction of the data entered.

$$R^2 = 1 - \left(\frac{\sum_{i=1}^{N} \left(X_{sim,i} - X_i \right)^2}{\sum_{i=1}^{N} \left(X_i - X_{ave} \right)^2} \right) \quad (15)$$

where X_{ave} indicates the average of the data in the thermodynamic model.

3. Results

3.1. Fuzzy Logic

Figures 8–17 show the membership functions of as well as the universe of speech for each input and output variable.

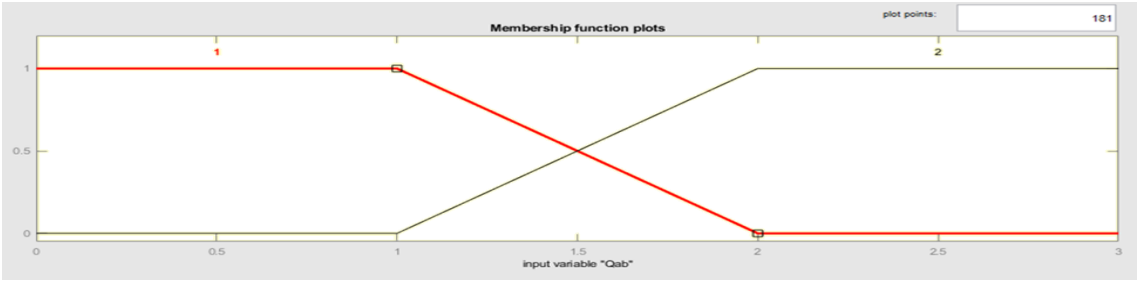

Figure 8. Membership functions of the input variable Q_{AB} [kW].

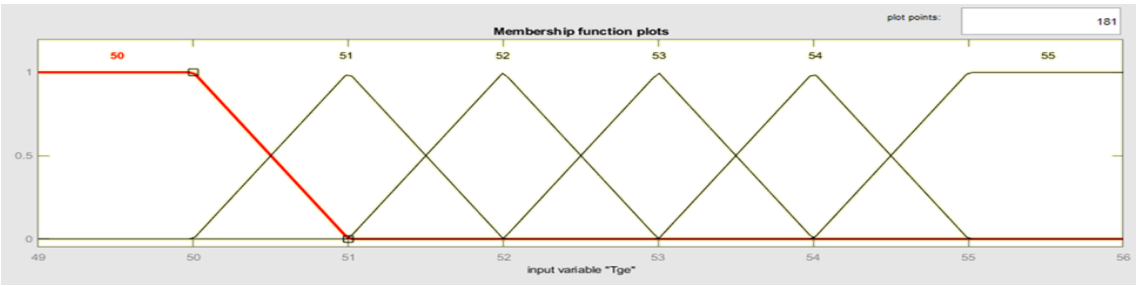

Figure 9. Membership functions of the input variable T_{GE} [°C].

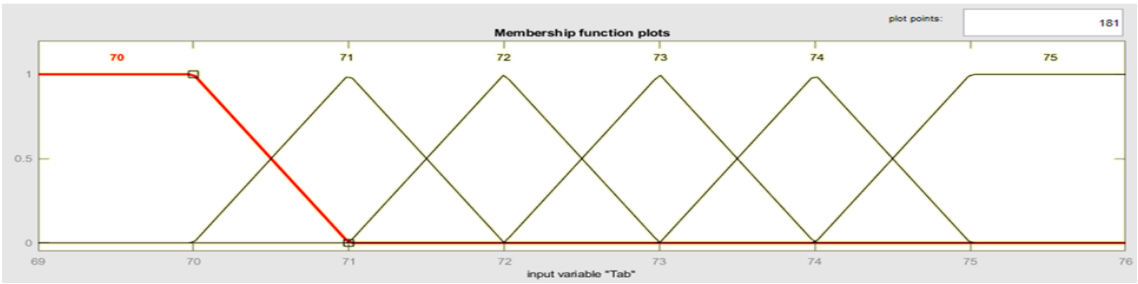

Figure 10. Membership functions of the input variable T_{AB} [°C].

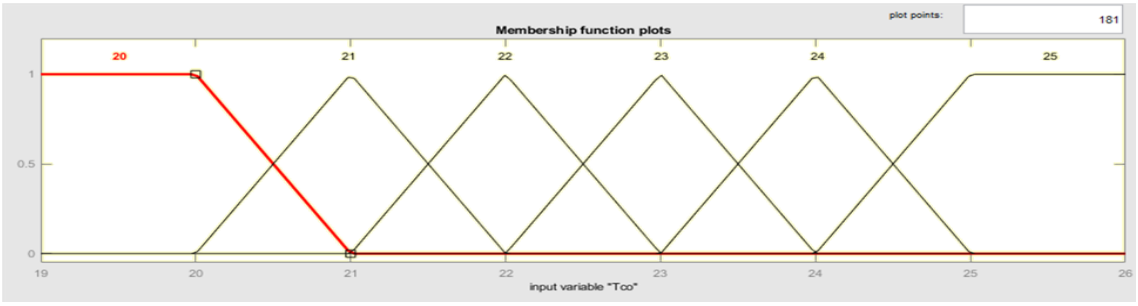

Figure 11. Membership functions of the input variable T_{CO} [°C].

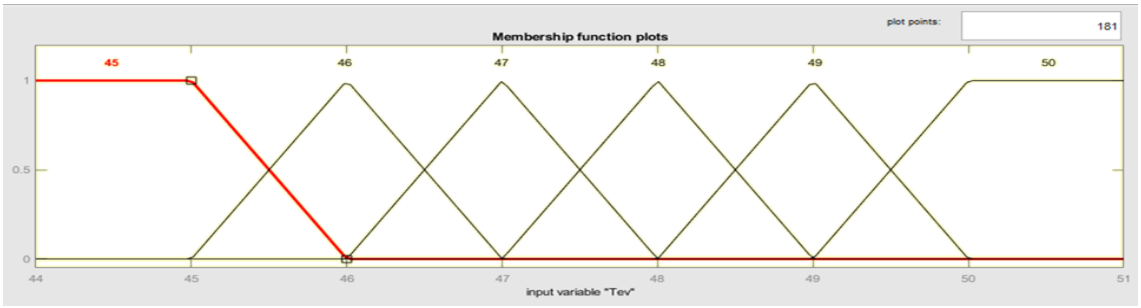

Figure 12. Membership functions of the input variable T_{EV} [°C].

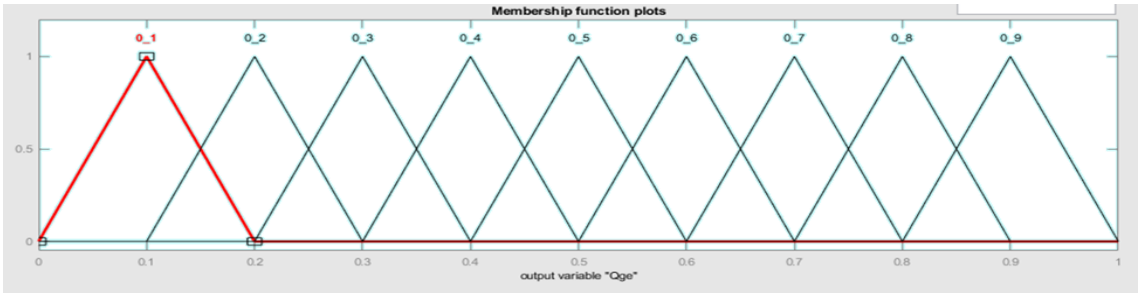

Figure 13. Membership functions of the output variable Q_{GE} [kW].

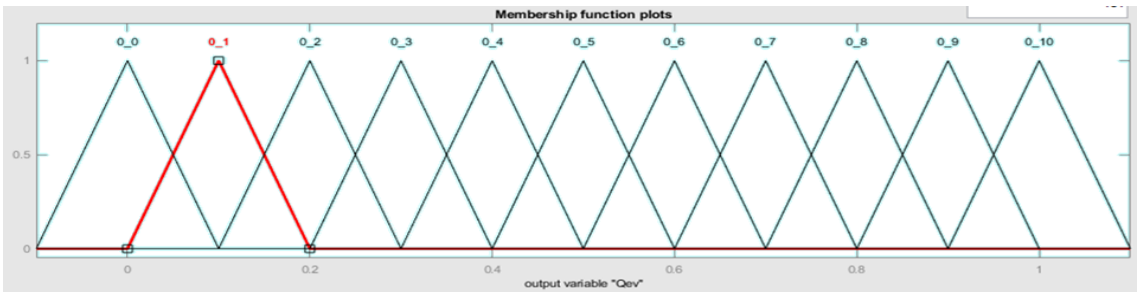

Figure 14. Membership functions of the output variable Q_{EV} [kW].

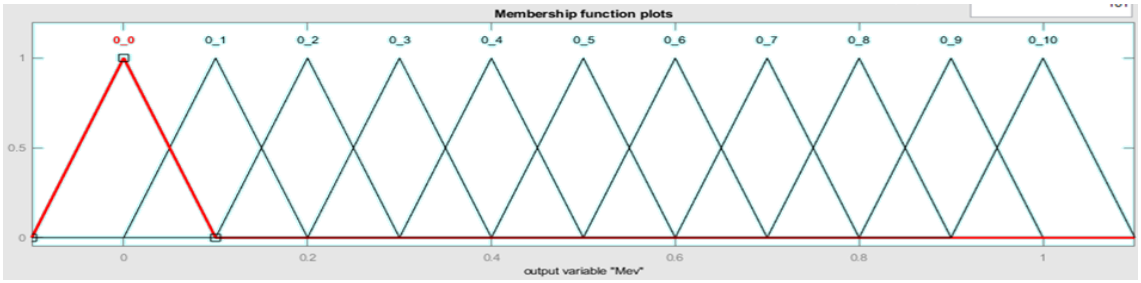

Figure 15. Membership functions of the output variable M_{EV} [kg/s].

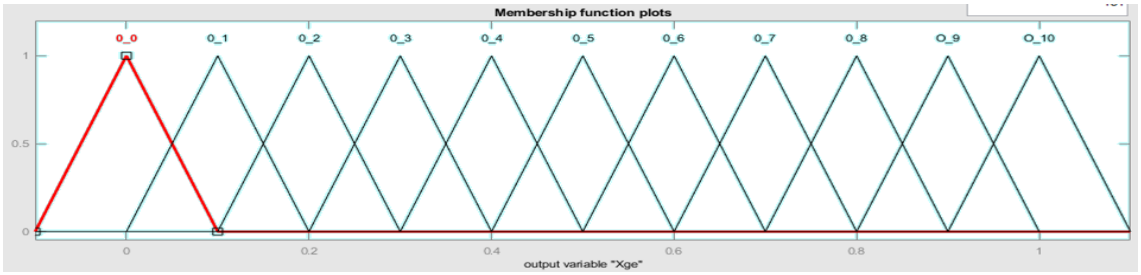

Figure 16. Membership functions of the output variable X_{GE} [%w].

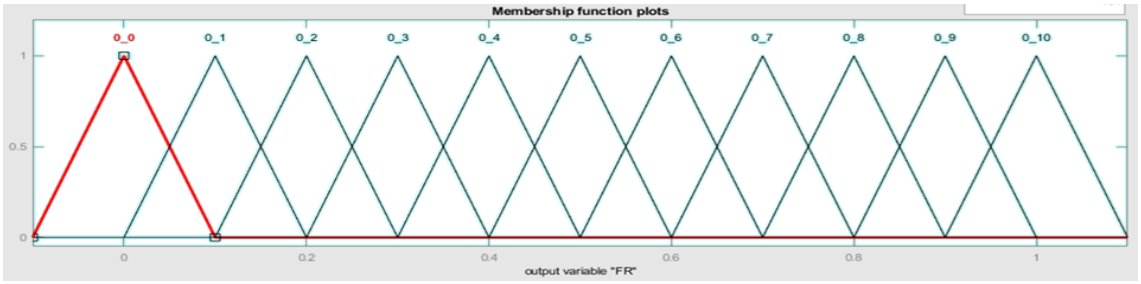

Figure 17. Membership functions of the FR [Dimensionless] output variable.

Fuzzy Logic Output

In Figure 18, an example of the output of the program execution in MATLAB can be seen for the Absorber power (Q_{AB}) entered by the user of 1 (kW) with operating conditions of generation at 50 °C, absorption at 70 °C; theoretically, the environment and condensate temperature are the same, which is 20 °C; and the steam in the Evaporator varies—in this case (of Figure 18), it is presented for the temperature of 47.5 °C. This Evaporator value changes, as it has been trained with thermodynamic data. The results obtained by the program are as follows: normalized generation power of 0.6 (maximum value 1.0095 kW and minimum 0.9969 kW), normalized evaporation power of 0.4 (maximum value 1.4904 kW and minimum 1.0798 kW), normalized evaporation mass flow (M_{EV}) of 0.3 (maximum value 0.00059 kg/s and value minimum 0.00043 kg/s), normalized concentration of the desorber or Generator of 0.5 (of a maximum value 56.6885 and minimum value 50.9332 in concentration kg of lithium bromide/kg of aqueous solution) and normalized flow ratio (FR) of 0.3 (with maximum values of 19.9291 and minimum 7.9601).

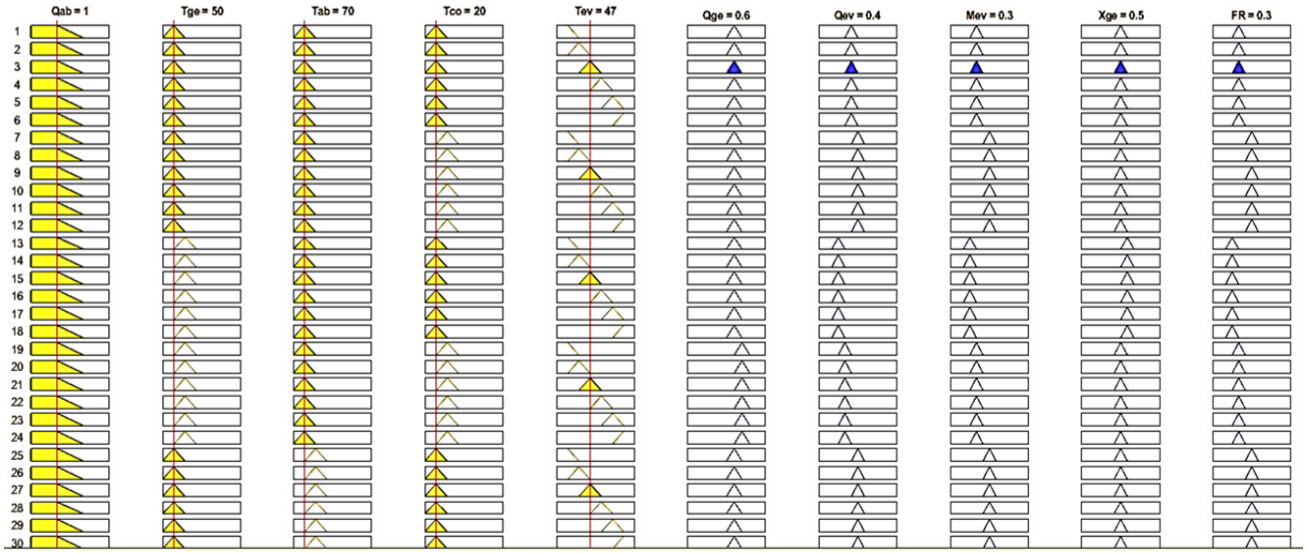

Figure 18. Select part of active rules according to the conditions of input variables, FIS.

3.2. Computational Model Based on Neural Networks

Based on the search for a value of R^2 that correlates with a value greater than 0.99, hidden layers from 5 to 25 were tested and, in layer 15, a value higher than the established criterion was obtained. According to the set of inputs and outputs shown in Figure 19, the Neural Network is shaped as shown below.

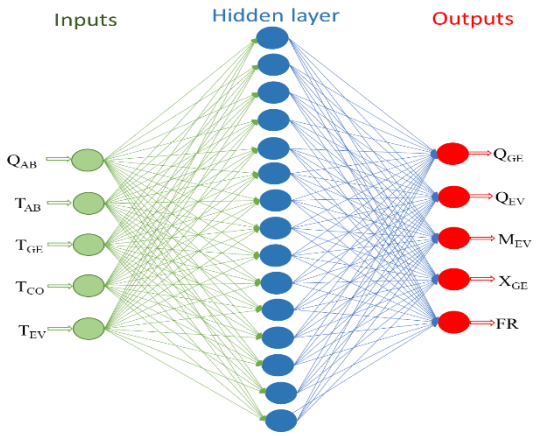

Figure 19. Model of the Neural Network perceptron multilayers.

ANN involved fifteen neurons (Ns = 15) in the hidden layer, 150 weights (Wi{k,s} = 75 (Table 4) and Wo{l, s} = 75 (Table 5)) and two biases, with 15 values for b1 and 5 values for b2 (Table 6); it was used to predict output values corresponding to the largest product of the values COP multiplied by GTL for a vector of conditions in the input values in the AHT in a stage.

Table 4. The weights of the input vector with respect to the hidden ANN layer of SSHT.

$\mathbf{Wi}_{\{15,1\}}$	$\mathbf{Wi}_{\{15,2\}}$	$\mathbf{Wi}_{\{15,3\}}$	$\mathbf{Wi}_{\{15,4\}}$
−0.9772	1.0564	0.0028	0.9100
−0.8625	0.9215	0.0023	0.8501
−1.8420	0.0977	−0.0015	0.0508
0.0659	−0.0879	5.2562×10^{-05}	0.0005
2.738	−0.0891	0.0024	−0.0348
−2.8736	2.8472	−0.0023	2.9076
−5.1080	4.7151	0.0136	0.6338
−2.8530	2.8258	−0.0023	2.8669
3.2812	0.0902	−0.0128	0.0313
−1.4776	1.0950	0.0046	1.3413
−1.2590	1.2930	−0.0004	−4.1966
5.1733	−3.9671	0.0010	8.2166
7.0039	−4.6306	0.0016	10.3212
−0.3480	0.0873	0.00163	0.07205
0.4706	−0.3563	0.0024	−0.4261

Table 5. The weights of the hidden layer relative to the SSHT ANN output vector.

$\mathbf{Wo}_{\{1,15\}}{}^{\mathbf{T}}$	$\mathbf{Wo}_{\{2,15\}}{}^{\mathbf{T}}$	$\mathbf{Wo}_{\{3,15\}}{}^{\mathbf{T}}$	$\mathbf{Wo}_{\{4,15\}}{}^{\mathbf{T}}$	$\mathbf{Wo}_{\{5,15\}}{}^{\mathbf{T}}$
−0.0617	−0.3965	−0.4247	0.0330	−1.7513
0.3548	0.8390	0.8682	−0.0196	2.5417
−0.4964	0.7147	0.6889	−0.2471	1.3084
0.4323	1.4499	1.1029	6.3634	−0.2043
−0.3122	0.5054	0.4899	−0.1723	0.9649
0.6374	1.1215	1.1160	−0.0060	1.3384
−0.0093	−0.0277	−0.0276	0.0089	−0.0331
−0.5772	−0.9895	−0.9849	0.0087	−1.1827
−0.0203	0.0717	0.0704	−0.0282	0.1246
−0.0419	0.0776	0.0724	−0.0026	−0.1485
0.6938	1.9976	1.9828	−0.0212	2.0050
0.9950	2.9670	2.9479	−0.0706	2.9920
−0.8368	−2.5002	−2.4841	0.0658	−2.5215
−1.3667	0.6120	0.5176	−0.4386	−0.1777
0.7445	−0.2982	−0.2779	−0.2779	0.3307

Table 6. Bias of the SSHT ANN model.

b1	**b2**
1.4210	−0.5270
1.2001	1.3199
1.3380	1.3343
0.2503	−1.7314
−1.8645	0.6977
0.8053	
−0.4996	
0.5853	
−0.0174	
0.1084	
−7.3954	
14.8259	
18.5230	
−0.7086	
0.7127	

During the network training period, the number of neurons in the hidden layer was varied to find the smallest MSE values for training, validation and testing. With the help of the trial and error method, the smallest MSE of training, validation and testing was found to be 34.00×10^{-05}, 3.16×10^{-05} and 3.01×10^{-05},respectively, for 15 neurons in the hidden layer. It has also been observed that the training performance of the network deteriorates when the number of neurons in the hidden layer is greater than 22 or less than 5.

These small MSE values indicate that network performance is good for predicting maximum COP product values per GTL for each operating condition of the input values. Regression plots are also used to validate network performance and show that the fit is reasonably good for all datasets, with regression values (R) in each case greater than 0.999 (Figure 20).

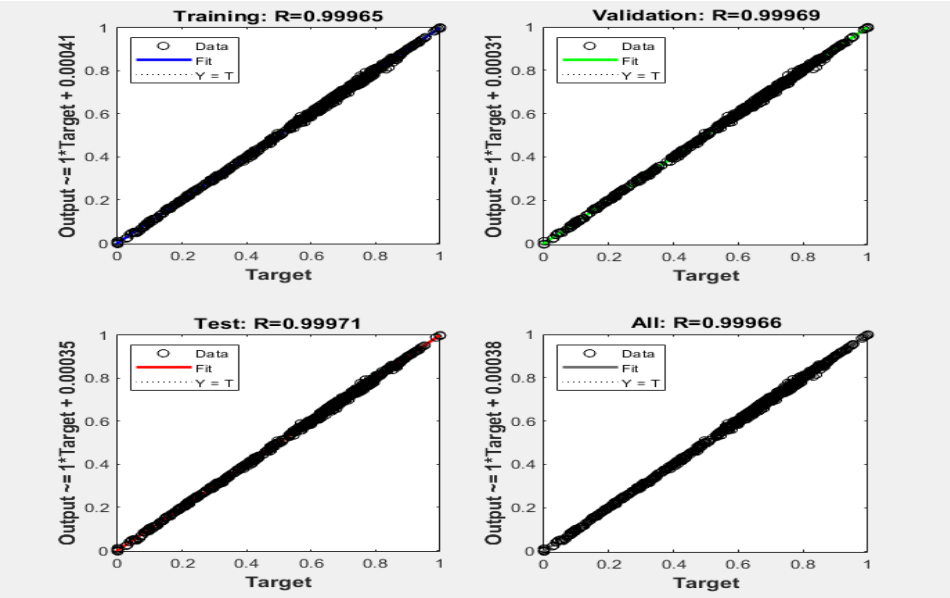

Figure 20. Network regression plot proposed for a stage.

Once the network has been trained with R^2 values of 0.9902 and MSEs of 3.34×10^{-05}, 3.16×10^{-05} and 3.01×10^{-05} for training, validation and testing, respectively, a MATLAB Simulink model of that network is created that simulates the outputs for any given input vector for the first stage.

3.3. Comparison of Both Computational Models

For the comparison of both models studied, the goodness adjustment indicators described above were used. Regarding the indicators of % Deviation, RMBE and MBE, lower values indicate better goodness-of-fit between the two methods; for the case of R^2, if the value is closer to 1, the fit of the model will be more accurate. Table 7 shows the different goodness-of-fit indicators used in the analysis of computational models based on Fuzzy Logic and Neural Networks.

Table 7. Comparison of computational models according to different indicators of goodness-of-fit (Equations (12)–(15)).

Fuzzy Logic	% Dev (max)	RMSE	MBE	R^2
Q_{GE}	0.145456403	4.20×10^{-04}	1.76×10^{-07}	0.974810
Q_{EV}	1.755065786	1.21×10^{-02}	1.45×10^{-04}	0.984409
M_{EV}	1.830934034	4.81×10^{-06}	2.32×10^{-11}	0.984793
X_{GE}	1.008901078	1.39×10^{-01}	1.93×10^{-02}	0.989974
FR	6.665546516	3.36×10^{-01}	1.13×10^{-01}	0.977917
Neural Networks	**% Dev (max)**	**RMSE**	**MBE**	**R^2**
Q_{GE}	0.014784	3.10×10^{-05}	9.61×10^{-10}	0.99986541
Q_{EV}	0.754447	2.94×10^{-03}	8.66×10^{-06}	0.99903313
M_{EV}	0.758600	1.18×10^{-06}	1.39×10^{-12}	0.99903697
X_{GE}	0.087526	0.18×10^{-01}	0.03×10^{-02}	0.99981534
FR	1.749315	0.80×10^{-01}	1.64×10^{-02}	0.99872625

Both programs present, for each output variable, values close to zero for the RMSE and MBE indicators, the % Deviation for the Fuzzy Logic program presents a maximum value of 6.7% and, for the ANN, the maximum deviation is 4.8%, with a maximum R^2 of 0.9998 for the ANN while, for the program of Fuzzy Logic, a range of 0.974 to 0.989 was obtained. The results show in both cases the similarity of the data for each output of the AI computer programs compared with the thermodynamic model. Therefore, in this work, it is proposed to use an ANN model for future applications of automatic control of double-stage absorption cycles with the following network.

3.4. ANN for DSHT

The AI of ANN for a double stage assumes that the first stage is operating with a maximum value of the product of COP_{SSHT} multiplied by GTL_{SSHT} and has, as the power to the second ANN, the condition $T_{AB2} = T_{EV1}$ (Figure 21). This ANN involved thirty neurons (Ns = 30) in the hidden layer [150 additional weights (Wi{k,s} = 75 (Table 8) and Wo{l, s} = 75 (Table 9)) and two biases with the following values: 15 new values for b1 and 5 new values for b2 (Table 10)]. It was used to predict the output values corresponding to the largest product of COP multiplied by GTL for a vector of conditions in the input values in the AHT in each stage.

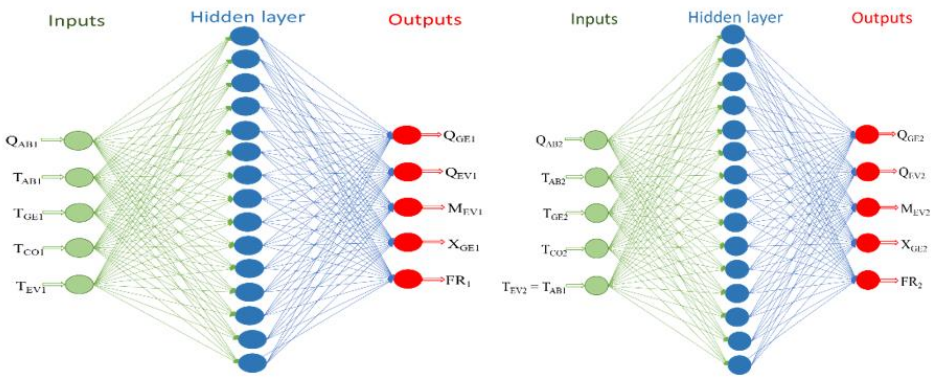

Figure 21. ANN for Double-Stage Heat Transformer.

Table 8. Weights of the input vector with respect to the hidden layer for DSHT ANN.

$\mathbf{Wi}_{\{15,1\}}$	$\mathbf{Wi}_{\{15,2\}}$	$\mathbf{Wi}_{\{15,3\}}$	$\mathbf{Wi}_{\{15,4\}}$
1.2254	−1.1448	0.0041	−1.1835
−0.2686	0.1965	−0.0033	0.2173
−0.0985	0.1185	0.0011	−0.0361
3.6820	−3.7613	0.0221	−3.2992
8.8366	−8.2592	0.0008	−1.8098
8.7259	−4.7289	0.0029	−13.2845
−7.8608	7.3009	−0.0025	1.11581
−8.4505	4.6515	−0.0014	11.6971
0.1140	0.2041	−0.0012	−0.1426
5.4186	−6.5799	−0.0012	0.9792
4.1579	−4.1439	−0.0180	−4.2200
−0.6326	1.4982	9.2773×10^{-05}	−0.8332
−6.6486	7.8499	0.0007	−0.9245
3.4092	2.0946	−0.0843	−2.9217
−0.2114	0.4584	0.0040	−0.2386

Table 9. The weights of the hidden layer with respect to the output vector for DSHT ANN.

$\mathbf{Wo}_{\{1,15\}}{}^{\mathbf{T}}$	$\mathbf{Wo}_{\{2,15\}}{}^{\mathbf{T}}$	$\mathbf{Wo}_{\{3,15\}}{}^{\mathbf{T}}$	$\mathbf{Wo}_{\{4,15\}}{}^{\mathbf{T}}$	$\mathbf{Wo}_{\{5,15\}}{}^{\mathbf{T}}$
−0.0731	−0.0966	−0.0981	0.0118	−0.3688
−0.4621	−0.2239	−0.2244	−0.6377	−0.7501
−3.1999	4.5836	4.5869	−3.4430	5.6008
0.0547	−0.1547	−0.1556	0.0085	−0.3077
-0.5996	1.0522	1.0544	−0.0376	1.2139
−2.3424	3.7439	3.7407	0.0026	2.8558
−0.6385	1.0985	1.1005	−0.0551	1.2548
−2.4679	3.9277	3.9244	−0.0062	3.0078
−0.0151	0.7491	0.7735	−0.2024	1.2248
−3.2268	4.5012	4.5002	−0.0953	3.3789
−0.0011	−0.0656	−0.0660	−0.0058	−0.1561
0.0925	−0.1877	−0.1882	0.0196	−0.2502
−3.1084	4.3051	4.3041	−0.0931	3.1681
0.0070	0.0088	0.0097	−0.0021	0.0165
0.6520	−1.2756	−1.2773	0.0292	−1.6757

Table 10. Values of bias 1 and bias 2 for ANN of DSHT.

b1	b2
−2.2891	−0.2966
0.0377	0.7999
−0.1885	0.8097
6.4594	−0.6725
12.8104	1.3759
20.5034	
−11.3639	
−18.7434	
−0.3747	
10.3655	
−3.9339	
−1.1616	
−12.3745	
3.31736	
0.3744	

In this ANN, the neurons were not varied and it was the consideration that the number of neurons of the ANN for a single stage should correspond to the same thermodynamic model that led to an ANN of 15 neurons. The value of R for training was calculated at 0.99965 (see Figure 22), which was higher than that of the first stage. In the case of training, the MSE value was 5.16×10^{-05}, for validation it was 4.55×10^{-05} and for testing 4.92×10^{-05}, which are lower than those obtained in the ANN for first stage AHT.

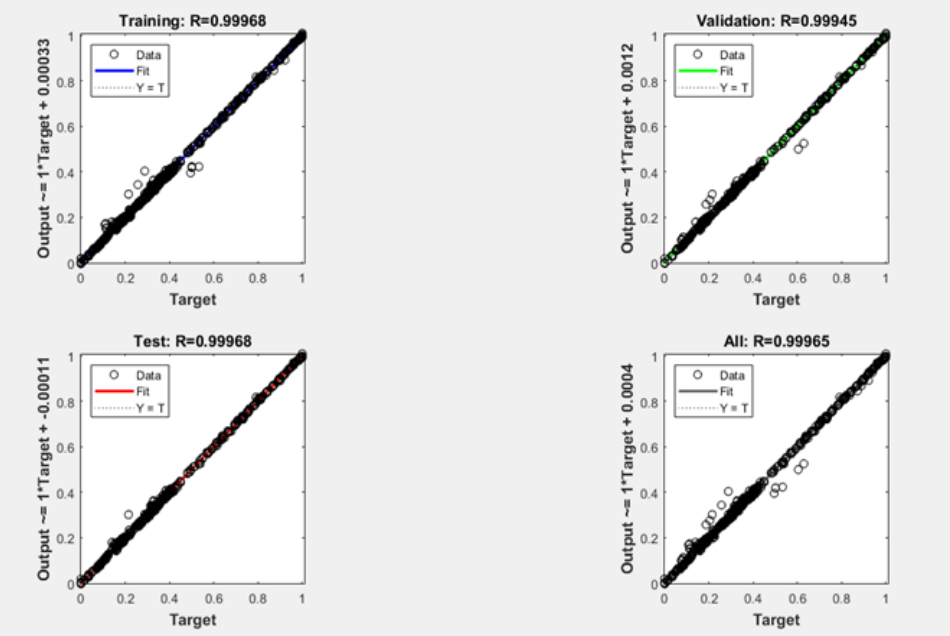

Figure 22. Values of R^2 for thermodynamic and calculated data of a DSHT.

Table 11 shows the different goodness adjustment indicators used in the ANN analysis for a double-stage AHT.

Table 11. Goodness-of-fit indicators for the ANN of a DSHT.

Neural Networks	% Error (max)	RMSE	MBE	R^2
Q_{GE2}	0.067516255	1.40×10^{-04}	1.95×10^{-08}	0.999467773
Q_{EV2}	4.168673681	1.55×10^{-02}	2.39×10^{-04}	0.999441275
M_{EV2}	4.202766596	6.23×10^{-06}	3.88×10^{-11}	1.000000000
X_{GE2}	0.128334019	2.32×10^{-02}	5.39×10^{-04}	0.999999808
FR_2	3.983523963	1.47×10^{-01}	2.18×10^{-02}	0.999712526

4. Discussion

Three AI computer programs have been programmed for the data leading to the highest value of the COP_{DSHT} multiplied by GTL_{DSHT} product as a strategy for calculating the conditions in which the highest absorption temperature is obtained without having the lowest COP as shown in Figure 3 inside the desired zone. There exists a vector of five output variables that would be the conditions in which an absorption cycle of a DSHT is operated for the greatest recovery of heat, whether from industrial, geothermal or solar waste. The programming for the FL AI has the inconvenience of arrangement of data with a normalization based on the lowest and largest values for each parameter. The member functions must be made accurate for each discourse universe of the variable. Every rule must be tested and interpreted by experts in the scientific field to be realistic and accurate with the physical process. For ANN AI, in this work, 70% of the thermodynamic data was used for training, 15% was used for testing and 15% was used for validation. The number of hidden layer neurons was specified as 5, 10, 15 and 20 as the methodology indicates, and

the best accuracy was 15. A Levenberg–Marquardt training algorithm was selected based on the time of data convergence.

After programming AI with Fuzzy Logic and programming AI with ANN, they were compared and it was observed that ANN can obtain higher values of goodness adjustment in the training, validation and testing phases of the calculated values with the values provided by a previously published thermodynamic model [54], that is, the nonlinear behavior process.

From the comparison of the AIs for the modeling of thermodynamic data of a single-stage AHT, the third AI has been programmed with ANN to calculate the conditions of the greater COP_{DSHT} multiplied by GTL_{DSHT} product with the future objective of implementing in real-time a cycle with these conditions by modifying the flow in the Evaporator. This flow has values from 0.000495732 to 0.001245909 kg/s for an Evaporator power from 1.260239935 to 3.151855192 kW. So, the ratio of flow/power for the Evaporator process goes from 0.0003933 kg/kJ to 0.0003952 kg/kJ.

5. Conclusions

FL and ANN of the AI derived from the analysis were compared, and the values of the goodness-of-fit greater than 0.9 were calculated in both cases, so they can be candidates to efficiently calculate the data previously reported for the operation of a thermal transformer by absorption of single and double stages operating with the mixture of lithium bromide–water.

The ANN AI has a value of $R^2 = 0.9990$ for the values of M_{EV} in the first stage AHT and the FL AI has a value of $R^2 = 0.9847$. The M_{EV} is an independent output variable that allows the control of the thermal power of the Evaporator; so, the ANN AI has been selected to calculate the operating conditions of DSHT, which include the X_{GE}, Q_{GE} and Q_{EV} for both stages. This strategy has not been proposed before.

The second AI of ANN has been generated for the double-stage that calculates the integration of the energy of the first stage to the second stage by the restriction $T_{AB2} = T_{EV1}$, with which a complete AI of 30 neurons, 300 weights and 40 biases was able to calculate the operating conditions for the highest value of COP_{DSHT} multiplied by $GTL_{DSHT.}$

The MRSE and MBE values for the M_{EV2} were 6.23×10^{-06} and 3.88×10^{-11}, respectively, so this AI-based control strategy is a potential candidate for the control of a Double-Stage Heat Transformer operating with a water–lithium bromide mixture.

The future work for this research will take the ANN AI, because the goodness-of-fit is better compared with the fuzzy technique. In the physical device, the flow ratio value must be correlated with the Evaporator flow with values calculated as a function of the absorption process in the second stage.

Author Contributions: Conceptualization, S.V.-A. and R.J.R.; Methodology, S.V.-A., M.M.-G. and J.C.; Software, S.V.-A.; Validation, S.V.-A., R.J.R. and J.C.; Formal analysis, S.V.-A., R.J.R., M.M.-G. and J.C.; Investigation, S.V.-A., R.J.R., M.M.-G. and J.C.; Resources, S.V.-A. and R.J.R.; Data curation, R.J.R.; Writing—original draft, S.V.-A.; Writing—review & editing, R.J.R., M.M.-G. and J.C.; Visualization, S.V.-A.; Supervision, R.J.R. All authors have read and agreed to the published version of the manuscript.

Funding: Consejo Nacional de Ciencia y Tecnología: CVU 9391109.

Conflicts of Interest: The authors declare no conflict of interest.

References

1. IEA. International Energy Agency. Available online: https://www.iea.org/reports/energy-technology-perspectives-2023 (accessed on 6 February 2023).
2. IEA. International Energy Agency World Energy Outlook. 2022. Available online: https://www.iea.org/reports/world-energy-outlook-2022 (accessed on 9 December 2022).
3. Oyepedo, S.O.; Fakeye, B.A. Waste heat recovery technologies: Pathway to sustainable energy development. *J. Therm. Eng.* **2021**, *7*, 324–348.
4. Romero, R.J.; Cerezo, J.; Rodriguez-Martinez, A.; Montiel, M. Absorption Heat Transformer for Solar Pond Energy Temperature Upgrading. *Chem. Eng. Trans.* **2021**, *86*, 703–708.

5. Wang, H.; Li, H.; Wang, L.; Bu, X.; Zeng, J.; Xie, N.; Xu, Q. A solar-assisted double absorption heat transformer: Off-design performance and optimum control strategy. *Energy Convers. Manag.* **2019**, *196*, 614–622. [CrossRef]
6. Cudok, F.; Giannetti, N.; Ciganda, J.L.C.; Aoyama, J.; Babu, P.; Coronas, A.; Ziegler, F. Absorption heat transformer-state-of-the-art of industrial applications. *Renew. Sustain. Energy Rev.* **2021**, *141*, 110757. [CrossRef]
7. Yari, M.; Salehi, S.; Mahmoudi, S.M.S. Three-objective optimization of water desalination systems based on the double-stage absorption heat transformers. *Desalination* **2017**, *405*, 10–28. [CrossRef]
8. Huicochea, A.; Siqueiros, J.; Romero, R.J. Portable water purification system integrated to a heat transformer. *Desalination* **2004**, *165*, 385–391. [CrossRef]
9. Huicochea, A.; Siqueiros, J. Increase of COP for an experimental heat transformer using a water purification system. *Desalination Water Treat* **2009**, *12*, 305–312. [CrossRef]
10. Huicochea, A.; Siqueiros, J. Improved efficiency of energy use of a heat transformer using a water purification system. *Desalination* **2010**, *257*, 8–15. [CrossRef]
11. Rivera, W.; Huicochea, A.; Martínez, H.; Siqueiros, J.; Juarez, D.; Cadenas, E. Exergy analysis of an experimental heat transformer for water purification. *Energy* **2011**, *36*, 320–327. [CrossRef]
12. Sekar, S.; Saravanan, R. Experimental studies on absorption heat transformer coupled distillation system. *Desalination* **2011**, *274*, 292–301. [CrossRef]
13. Huicochea, A.; Rivera, W.; Martínez, H.; Siqueiros, J.; Cadenas, E. Analysis of the behavior of an experimental absorption heat transformer for water purification for different mass flux rates in the generator. *Appl. Therm. Eng.* **2013**, *52*, 38–45. [CrossRef]
14. Meza, M.; Marquez-Nolasco, A.; Huicochea, A.; Juarez-Romero, D.; Siqueiros, J. Experimental study of an absorption heat transformer with heat recycling to the generator. *Exp. Therm. Fluid Sci.* **2014**, *53*, 171–178. [CrossRef]
15. Cortés, E.; Rivera, W. Exergetic and exergoeconomic optimization of a cogeneration pulp and paper mill plant including the use of a heat transformer. *Energy* **2010**, *35*, 1289–1299. [CrossRef]
16. Horus, I.; Kurt, B. Absorption heat transformers and an industrial application. *Renew. Energy* **2010**, *35*, 2175–2181. [CrossRef]
17. Rivera, W.; Best, R.; Cardoso, M.J.; Romero, R.J. A review of absorption heat transformers. *Appl. Therm. Eng.* **2015**, *91*, 654–670. [CrossRef]
18. Romero, R.; Rodriguez-Martinez, A.; Cerezo, J.; Rivera, W. Comparison of Double Stage Heat Transformer with Double Absorption Heat Transformer Operating with Carrol—Water for Industrial Waste Heat Recovery. *Chem. Eng. Trans.* **2011**, *25*, 129–134.
19. Rivera, W.; Cerezo, J.; Rivero, R.; Cervantes, J.; Best, R. Single stage and double absorption heat transformers used to recover energy in a distillation column of butane and pentane. *Int. J. Energy Res.* **2003**, *27*, 1279–1292. [CrossRef]
20. Ma, X.; Chen, J.; Li, S.; Sha, Q.; Liang, A.; Li, W.; Zhang, J.; Zheng, G.; Feng, Z. Application of absorption heat transformer to recover waste heat from a synthetic rubber plant. *Appl. Therm. Eng.* **2003**, *23*, 797–806. [CrossRef]
21. Fujii, T.; Kawamura, H.; Uchida, S.; Nishiguchi, A. A single-effect absorption heat transformer for waste heat recovery in industrial use. In Proceedings of the 9th International IEA Heat Pump Conference, Zürich, Switzerland, 20–22 May 2008; Conference Proceedings Paper; International Energy Agency: Paris, France, 2008.
22. Fujii, T.; Uchida, S.; Nishiguchi, A. Development Activities of Low Temperature Waste Heat Recovery Appliances using Absorption Heat Pumps. In Proceedings of the International Symposium on Next-Generation Air Conditioning and Refrigeration Technology, Tokyo, Japan, 17–19 February 2010.
23. Parham, K.; Khamooshi, M.; Daneshvar, S.; Assadi, M.; Yari, M. Comparative assessment of different categories of absorption heat transformers in water desalination process. *Desalination* **2016**, *396*, 17–29. [CrossRef]
24. Vázquez-Aveledo, S.; Diaz-Gonzalez, L.; Montiel-Gonzalez, M.; Romero, R.J. Risk of Overwarming for Flow Variation into an Absorption Heat Transformer for Waste Heat Recovery Process. *Chem. Eng. Trans.* **2022**, *91*, 373–378.
25. Rivera, W.; Romero, R.; Cardoso, M.J.; Aguillón, J.; Best, R. Theoretical and experimental comparison of the performance of a single-stage heat transformer operating with water/lithium bromide and water/Carrol. *Int. J. Energy Res.* **2002**, *26*, 747–762. [CrossRef]
26. Hdz-Jasso, A.M.; Contreras-Valenzuela, M.R.; Rodríguez-Martínez, A.; Romero, R.J.; Venegas, M. Experimental heat transformer monitoring based on linear modelling and statistical control process. *Appl. Therm. Eng.* **2015**, *75*, 1271–1286. [CrossRef]
27. Goyal, A.; Staedter, M.A.; Garimella, S. A review of control methodologies for vapor compression and absorption heat pumps. *Int. J. Refrig. Rev. Int. Du Froid* **2018**, *97*, 1–20. [CrossRef]
28. Broersen, P.M.T.; Van Der Jagt, M.F.G. Hunting of Evaporators Controlled by a Thermostatic Expansion Valve. *J. Dyn. Syst. Meas. Control.* **1980**, *102*, 130–135. [CrossRef]
29. Gruhle, W.D.; Isermann, R. Modeling and Control of a Refrigerant Evaporator. *J. Dyn. Syst. Meas. Control.* **1985**, *107*, 235–240. [CrossRef]
30. Qureshi, T.Q.; Tassou, S.A. Variable-Speed Capacity Control in Refrigeration Systems. *Appl. Therm. Eng.* **1996**, *16*, 103–113. [CrossRef]
31. Marcinichen, J.B.; Holanda, T.N.D.; Melo, C.A. Dual Siso Controller for a Vapor Compression Refrigeration System. In Proceedings of the International Refrigeration and Air-Conditioning Conference, West Lafayette, IN, USA, 14–17 July 2008.
32. Li, X.; Chen, J.; Chen, Z.; Liu, W.; Hu, W.; Liu, X. A New Method for Controlling Refrigerant Flow in Automobile Air Conditioning. *Appl. Therm. Eng.* **2004**, *24*, 1073–1085. [CrossRef]

33. Ekren, O.; Sahin, S.; Isler, Y. Comparison of Different Controllers for Variable Speed Compressor and Electronic Expansion Valve. *Int. J. Refrig.* **2010**, *33*, 1161–1168. [CrossRef]
34. Rêgo, A.T.; Hanriot, S.M.; Oliveira, A.F.; Brito, P.; Rêgo, T.F.U. Automotive Exhaust Gas Flow Control for an Ammonia–Water Absorption Refrigeration System. *Appl. Therm. Eng.* **2014**, *64*, 101–107. [CrossRef]
35. Goyal, A.; Rattner, A.S.; Garimella, S. Model-Based Feedback Control of an Ammonia-Water Absorption Chiller. *Sci. Technol. Built Environ.* **2015**, *21*, 357–364. [CrossRef]
36. Zinet, M.; Rulliere, R.; Haberschill, A. Numerical Model for the Dynamic Simulation of a Recirculation Single-Effect Absorption Chiller. *Energy Convers. Manag.* **2012**, *62*, 51–63. [CrossRef]
37. Xu, Y.J.; Zhang, S.J.; Xiao, Y. Modeling the Dynamic Simulation and Control of a Single Effect H_2O-Libr Absorption Chiller. *Appl. Therm. Eng.* **2016**, *107*, 1183–1191. [CrossRef]
38. Garcíadealva, Y.; Best, R.; Hugo, H.; Vargas, A.; Rivera, W.; Jiménez-García, J.C. A Cascade Proportional Integral Derivative Control for a Plate-Heat-Exchanger-Based Solar Absorption Cooling System. *Energies* **2021**, *14*, 4058. [CrossRef]
39. Silva-Sotelo, S.; Romero, R.; Rodríguez-Martínez, A. Double Stage Heat Transformer Controlled by Flow Ratio. In *Innovations in Computing Sciences and Software Engineering*; Springer: Dordrecht, The Netherlands, 2009; pp. 577–581.
40. Santos, M. Un enfoque aplicado al control inteligente. *Rev. Iberoam. De Automática E Inf. Ind.* **2011**, *8*, 283–296. [CrossRef]
41. Valdez, V.; Romero, R. Optimal Design Criterion for Heat Transformer operating with Water Carrol. In Proceedings of the International Conference on Advanced in Mechanical and Atomation Engineering-MAE2016, Rome, Italy, 18–19 August 2016; SEEK Digital Library: New York, NY, USA, 2016; pp. 57–59.
42. Belman-Flores, J.M.; Rodríguez-Valderrama, D.A.; Ledesma, S.; García-Pabón, J.J.; Hernández, D.; Pardo-Cely, D.M. A Review on Applications of Fuzzy Logic Control for Refrigeration Systems. *Appl. Sci.* **2022**, *12*, 1302. [CrossRef]
43. Islam, M.A.; Hossain, M.S.; Haque, I.S.M. Mathematical Comparison of Defuzzification of Fuzzy Logic Controller for Intelligence Air Conditioning System. *Int. J. Sci. Res. Math. Stat. Sci.* **2021**, *8*, 29–37.
44. MathWork. Available online: https://es.mathworks.com/products/deep-learning.html (accessed on 17 March 2023).
45. Hooda, D.S.; Raich, V. *Fuzzy Logic Models and Fuzzy Control an Introduction*; Alpha Science International Ltd.: Oxford, UK, 2017; 408p.
46. Chandwani, V.; Agrawal, V.; Nagar, R. Modeling slump of ready mix concrete using genetic algorithms assisted training of Artificial Neural Networks. *Expert Syst. Appl.* **2015**, *42*, 885–893. [CrossRef]
47. Adil, O.; Ali, M.; Ali, A. Comparison between the Effects of Different Types of Membership Functions on Fuzzy Logic Controller Performance. *Int. J. Emerg. Eng. Res. Technol.* **2015**, *3*, 76–83.
48. Asanza, W.R.; Olivo, B.M. *Redes Neuronales Artificiales Aplicadas al Reconocimiento de Patrones*; UTMACH: Machala, Ecuador, 2018; pp. 11–35.
49. Villada, F.; Munoz, N.; García-Quintero, E. Redes Neuronales Artificiales aplicadas a la Predicción del Precio del Oro. *Inf. Tecnol.* **2016**, *27*, 143–150. [CrossRef]
50. Sayed, B.T.; Al-Mohair, H.K.; Alkhayyat, A.; Ramírez-Coronel, A.A.; Elsahabi, M. Comparing machine-learning-based black box techniques and white box models to predict rainfall-runoff in a northern area of Iraq, the Little Khabur River. *Water Sci. Technol.* **2023**, *87*, 812–822. [CrossRef]
51. Farzaneh-Gord, M.; Rahbari, H.R.; Mohseni-Gharesafa, B.; Toikka, A.; Zvereva, I. Accurate determination of natural gas compressibility factor by measuring temperature, pressure and Joule-Thomson coefficient: Artificial neural network approach. *J. Pet. Sci. Eng.* **2021**, *202*, 108427. [CrossRef]
52. Lugo, S.; Morales, L.I.; Best, R.; Gómez, V.H.; García-Valladares, O. Numerical simulation and experimental validation of an outdoor-swimming pool solar heating system in warm climates. *Sol. Energy* **2019**, *189*, 45–56. [CrossRef]
53. Rivera, W.; Romero, R.J.; Cardoso, M.J. Theoretical comparison of single stage and advanced absorption heat transformers operating with water/lithium bromide and water/carrol mixtures. *Int. J. Energy Res.* **1998**, *22*, 427–442. [CrossRef]
54. Hernández, J.A.; Romero, R.J.; Juárez, D.; Escobar, R.F.; Siqueiros, J. A neural network approach and thermodynamic model of waste energy recovery in a heat transformer in a water purification process. *Desalination* **2009**, *243*, 273–285. [CrossRef]